Probing Local Effects in Silica Sol−Gel Media by Fluorescence Spectroscopy of *p*-DASPMI

Ana Rei,*,† Graham Hungerford,†,‡ and Maria Isabel C. Ferreira†

Departamento de Física, Universidade do Minho, 4710-057 Braga, Portugal, and Physics Department, King's College London, Strand, London WC2R 2LS, U.K.

Received: February 14, 2008; Revised Manuscript Received: May 05, 2008

Stillbazolium salts present remarkable potential for application in several scientific areas. Their versatile behavior is explained by invoking the "twisted intramolecular charge-transfer" (TICT) mechanism, a model that describes the multiple fluorescence of DASPMI (4-(4-(dimethylamino)styryl)-*N*-methylpyridiniumiodine). One feature of their behavior is the sensitivity of the fluorescence lifetime to viscosity, thus identifying them as suitable probes for microheterogeneous systems, such as cells and sol−gel derived media. Because of their optical transparency, sol−gel matrices are light addressable and therefore appropriate for performing spectroscopic studies. The sol−gel process has been successfully used to produce hosts to biomolecules like proteins, for biosensor applications; however, these systems have to be optimized. Therefore, in this study modification of the matrices was performed through the incorporation of either silanes or polymers. (Aminopropyl)triethoxysilane, trimethoxypropylsilane, or (glycidyloxypropyl)triethoxysilane were added. The modification was also extended to the incorporation of the polymers poly(ethylene glycol) (molecular weight 300 and 20000) and Gelrite. The effect of these modifiers upon the gelation and aging processes was examined via the study of the photophysics of *p*-DASPMI by using both steady-state and time-resolved fluorescence. It was possible to discriminate the dominant dye−host interactions in each of the main steps of the preparation of modified sol−gel matrices.

1. Introduction

The association of fluorescent dyes with sol−gel derived media has been fruitful in several aspects. By choosing well-characterized fluorescent probes, it is possible to monitor the sol−gel process, as it is known that these materials undergo profound modifications during the sol−gel transition and the aging process.[1,2] A significant number of fluorescent probes have been employed to study sol−gel derived media.[3–5] Highly solvatochromic dyes, such as PRODAN[6,7] and Nile red[8,9] have been successfully applied to study both the number and polarity of local environments present within sol−gel derived media.[10,11] As well as obtaining information concerning the local polarity/dielectric constant, it is also important to understand the accessibility (transport processes) to biomolecules within the matrix, especially for biosensor applications. Various techniques can be employed to elucidate the ability of a molecule to diffuse (rotationally or translationally), such as fluorescence anisotropy[12] and fluorescence recovery after photobleaching (FRAP).[13] Both have been applied to sol−gel derived media,[14,15] and the authors have reported their combined use.[16,17] A further, very interesting, approach is the use of confocal microscopy to monitor the diffusion of single molecules within the sol−gel derived host.[18] Stilbenoid dyes are promising in that their photophysical properties are very sensitive to solvent viscosity.[19] The dye 4-(4-(dimethylamino)styryl)-*N*-methylpyridiniumiodine (*p*-DASPMI) has been commonly used to study cellular processes[20,21] and its decay time found to be dependent on viscosity,[22,23] with its multiple fluorescence ascribed to intramolecular charge transfer.[23] A related dye has also been used to study the course of gelation in the sol−gel reaction.[24,25] The authors have previously incorporated *p*-DASPMI into a sol−gel derived host and found a 100-fold increase in its lifetime[26] when compared with solution.[22]

In this work time-resolved and steady-state fluorescence measurements of *p*-DASPMI have been used to monitor the changes that occur in the preparation of sol−gel derived SiO_2 matrices (SGM) during the gelation and aging stages. These host materials were based on a previous reaction procedure using tetraethylorthosilicate (TEOS) to form a sol.[27] However, SGMs are not always ideal hosts for biomolecules. Therefore, in this study, modification of the matrices was performed through the incorporation of either silanes or polymers. (3-Aminopropyl-)triethoxysilane (APTES), trimethoxypropylsilane (TMPS), or (glycidyloxypropyl)triethoxysilane (GPTES) were added. The modification was also extended to the incorporation of the polymers poly(ethylene glycol) (PEG 20*k*, PEG 300) and Gelrite (GR), a commercial form of gellan gum. The effect of these modifiers upon the gelation and aging processes was examined via the study of the photophysics of *p*-DASPMI.

Whenever immersed in a medium, the photophysics of a fluorescent probe, *p*-DASPMI in the present study, inevitably reports on the medium's characteristics through its interaction with the surroundings. It is well-known that probe−host interactions are, in most cases, the result of: (a) electronic and/or dipolar relaxation events, expressed as solvatochromic shifts in the emission spectra; (b) hydrodynamic factors that arise from the probe mobility (translational and/or rotational), expressed by the influence of the viscosity of the host medium on the photophysics of the probe, particularly on the nonradiative decay processes; and (c) other specific interactions, largely dependent upon the nature of the probe and the host medium. In the present work the authors were able to discriminate the dominant dye−host interactions in each of the main steps of the

* Corresponding author. Phone: 00351-253604320. Fax: 00351-253678981. E-mail: anarei@fisica.uminho.pt.
† Universidade do Minho.
‡ King's College London.

10.1021/jp8013207 CCC: $40.75
Published on Web 06/28/2008

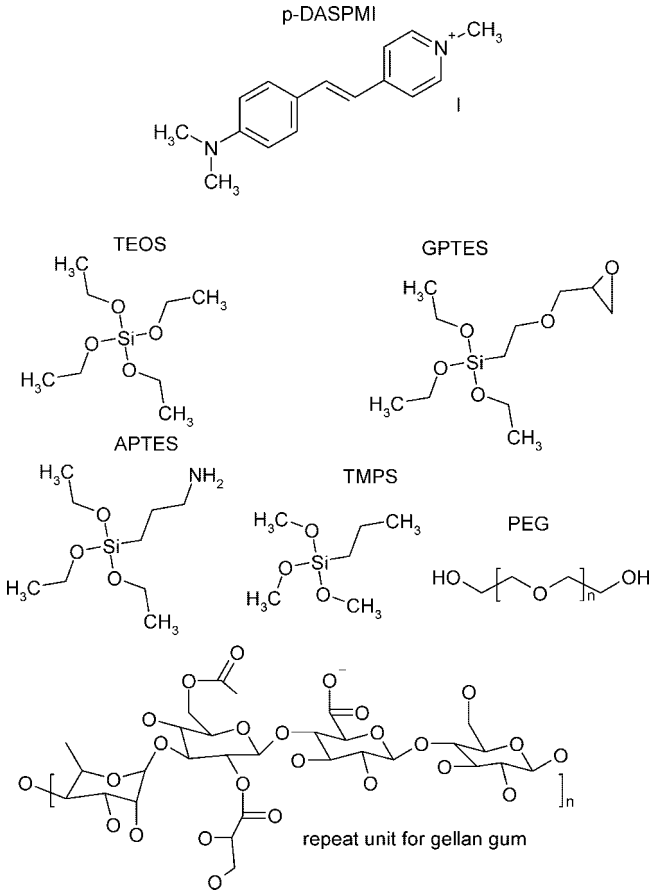

Figure 1. Structures of *p*-DASPMI, TEOS, and modifiers used to manufacture the matrices.

preparation of the SGMs, as reported by the study of the photophysics of *p*-DASPMI throughout the preparation and aging of those matrices.

2. Experimental Section

2.1. Sample Preparation. The dye *p*-DASPMI was purchased from Molecular Probes (Invitogen SA). The silanes TEOS, APTES, and TMPS and the polymers poly(ethylene glycol) (PEG 20*k*, PEG 300) and Gelrite (GR), a commercial form of gellan gum, were acquired from Aldrich. (3-Glycidyloxypropyl)triethoxysilane (GPTES) was from Fluka. All chemicals were used as received. The chemical structures of *p*-DASPMI, the silanes, and the polymers are shown in Figure 1. The phosphate buffer was adjusted to prepare aqueous solutions of pH 6, 7, and 8. Such a range of pH prevents protonation of *p*-DASPMI, as this can lead to a spectral change[23,26] that could compromise the intended objective of the present work, e.g., the study of the dye−host interactions for monitoring the sol−gel process.

The SGMs were prepared as previously reported,[17,27] on the basis of the method presented by Flora and Brennan.[10] The samples were manufactured using 10 mm polystyrene cuvettes (ca. 4.5 mL volume) by taking 2 mL of sol and adding the modifier, DASPMI (in water) and phosphate buffer (pH7, 2 mL). The cuvettes were then sealed, and the mixture was homogenized by shaking gently each sample. The solution gelled within minutes and was stored between measurements at 4 °C with the top of the cuvette covered with Parafilm. During the period of this experiment the matrices shrank, on average, to ca. 60% of their initial volume. Each matrix will be referred to by the matrix acronym (TEOS) and the acronym of the respective modifier (APTES, TMPS, etc). Therefore TEOS−APTES refers to a TEOS matrix modified by APTES. The quantity of each additive was chosen in order to produce samples with good optical quality. These quantities produced the following samples: 3.75% (v/v) TMPS or GTPES, 0.5% (v/v) APTES, 2.5% (v/v) PEG 300, 0.04 wt % PEG 20*k*, and 0.02 wt % GR. The transparent monoliths were allowed to warm to room temperature prior to measurement.

2.2. Measurements and Data Analysis. Absorption spectra were measured on a Shimadzu 3101 PC. Fluorescence and excitation spectra were recorded on a Fluorolog 3, from Horiba, Jobin Yvon. Difference spectra were calculated by normalizing the emission spectra at the maximum and subtracting from a reference spectrum taken for *p*-DASPMI just after gelation (day 0). These data were treated using Microcal Origin 7 software. Fluorescence quantum yields, ϕ_F, in solution were determined relative to *p*-DASPMI in ethanol, reported to be 0.008 by Rettig and Strehmel.[22] The optically dilute method was adopted,[28] and correction for the spectral response of the equipment was also made.

Time-resolved measurements used a single-photon counting apparatus equipped with a NanoLED excitation source emitting at 490 nm (HORIBA, Jobin Yvon, IBH Ltd. Glasgow, Scotland). The fluorescence emission was wavelength-selected using a 550 nm cutoff filter and detected with a Hamamatsu R2949 photomultiplier. Data analysis was performed with IBH DAS6 software and the goodness of fit judged in terms of a χ^2 value and weighted residuals. The decay time data were analyzed by using a sum of exponentials, employing a nonlinear least-squares reconvolution analysis of the form

$$I(t) = \sum_{i=1}^{n} \alpha_i \exp\left(\frac{-t}{\tau_i}\right) \tag{1}$$

where τ is the decay time. The preexponential factors (α_i) are given normalized to unity and errors given as three standard deviations. Average lifetimes, $\langle\tau\rangle$, were calculated as

$$\langle\tau\rangle = \sum_i \alpha_i \tau_i \tag{2}$$

Time-resolved fluorescence anisotropy measurements, $r(t)$, were performed by using linearly polarized light as the excitation source and measuring the fluorescence emission decays at polarizations parallel, $I_{||}(t)$, and perpendicular, $I_{\perp}(t)$, to that of the excitation, so that

$$r(t) = \frac{I_{||}(t) - GI_{\perp}(t)}{I_{||}(t) + 2GI_{\perp}(t)} \tag{3}$$

G corrects for the instrumental response (with the equipment used, this was 1). In the case of a spherical molecule $r(t)$ is related to the rotational correlation time, τ_r, according to

$$r(t) = (r_0 - r_\infty) \exp\left(-\frac{t}{\tau_r}\right) + r_\infty \tag{4}$$

with r_0 the initial anisotropy and r_∞ the limiting anisotropy. The rotational correlation time, τ_r, is related to the solvent viscosity, η, and the volume of a spherical rotating molecule, V, according to the well-known equation

$$\tau_r = \frac{\eta V}{kT} \tag{5}$$

where k is the Boltzmann constant and T is the absolute temperature. Measurements were taken over a 40 day period to

TABLE 1: Time-Resolved Fluorescence Decay Parameters of *p*-DASPMI in Glycerol−Water Mixtures

sample composition (wt % Gly)	τ_1 (ns)	τ_2 (ns)	τ_3 (ns)	α_1	α_2	α_3	χ^2	$\langle\tau\rangle$ (ns)
80	0.15 ± 0.11	0.37 ± 0.02		0.52	0.48		1.04	0.26
84	0.17 ± 0.10	0.46 ± 0.01		0.45	0.55		1.06	0.33
88	0.16 ± 0.17	0.57 ± 0.01		0.33	0.67		1.12	0.44
92	0.22 ± 0.08	0.75 ± 0.02	2.22 ± 0.40	0.29	0.70	0.01	1.20	0.60
96	0.27 ± 0.18	0.91 ± 0.04	1.77 ± 0.19	0.25	0.73	0.03	1.12	0.77
100	0.40 ± 0.06	1.25 ± 0.04	2.68 ± 0.58	0.28	0.71	0.01	1.10	1.03

check for longer term changes during sol−gel host aging. All measurements were made at room temperature. Hyperchem 7 molecular modeling software was used to estimate *p*-DASPMI characteristic dimensions and volume.

3. Results and Discussion

It is well-known that the preparation of SGM encompasses two major steps, gelation and aging. During the gelation process, extensive and profound chemical and physical changes occur, namely, the hydrolysis and the condensation of the silica network.[1] As a consequence, a drastic increase in viscosity occurs. Gelation, complex as it is, depends strongly upon many variables, such as the temperature, the nature, and the concentration of electrolytes, solvents, precursors, or any other chemical species present. During the aging process, polycondensation progresses with concomitant local solubilization and reprecipitation events, thereby causing a significant decrease in porosity and increase in mechanical strength.[1] Naturally the connectivity of the silica network increases substantially during this step. As the syneresis (shrinkage) occurs, an important fraction of liquid is expelled from the pores, thus providing a further change in the chemical composition of the liquid phase. The monitoring of such complex and fast processes is imperative whenever such matrices become hosts for biomolecules.

In this work the authors have studied the photophysics of *p*-DASPMI when incorporated into different modified and nonmodified SGMs, during gelation and aging, as will be described. In fact, stilbene dyes are an appropriate choice in that they display emission spectra that may arise from distinct configurations of the excited state, determined not only by the rotational mobility of the molecule but also by the internal charge-transfer character of the excited state.[19,22,23]

3.1. Preliminary Study on the Photophysics of *p*-DASPMI in Water−Glycerol Mixtures. Prior to the monitoring of SGM production, the authors performed a study on the photophysics of *p*-DASPMI in water−glycerol mixtures, containing different percentages of glycerol. Such mixtures were considered as appropriate models for the complex SGMs; in fact, glycerol possesses several OH groups (similarly to the SGMs), and water is also a relevant species in the synthesis of the matrices. All emission spectra, obtained upon excitation at 490 nm, showed one broad maximum centered at 600 nm and no structure. All decays were found to be multiexponential, in agreement with previous work.[19,22,23] Table 1 describes the fluorescence decay times obtained from the analysis of the time-resolved fluorescence of *p*-DASPMI. According to Rettig et al.,[23] the multiple fluorescence emission is related to different states: a planar excited state, originating directly from the $S_0 \rightarrow S_1$ transition, to which the lowest lifetime is ascribed (τ_1); a second emitting state, planar and most probably with a significant charge-transfer character (τ_2); and a third, the TICT state, e.g., a twisted intramolecular charge-transfer excited state, associated with the longest lifetime component (τ_3). Under the experimental conditions of the present work, components τ_1 and τ_2 dominate the observed decays. Only minute contributions ascribed to τ_3 could be found, with negligible physical significance. These results indicate that, most probably, the solvent cage surrounding the excited dye molecule may hinder the twisting of the molecule, thus precluding the formation of the TICT state. The "rigidity" of the solvent cage is a consequence of the hydrogen bonds that occur between the glycerol molecules and glycerol−water molecules.[29] This hypothesis is supported by further arguments presented in this section, when discussing the time-resolved fluorescence anisotropy data.

The average emission lifetime for each sample was obtained from the analysis of each fluorescence decay, according to eq 2. The radiative, (k_f) and nonradiative (k_{nr}) rate constants for *p*-DASPMI emission were then obtained from the well-known equations

$$k_f = \frac{\varphi_f}{\tau_f} \tag{6}$$

$$k_{nr} = \frac{(1-\varphi_f)}{\tau_f} \tag{7}$$

Since the emission decays were found to be multiexponential, the average emission lifetime was taken as τ_f in eqs 6 and 7. All results are shown in Table 2, where the refractive index (n) and the macroscopic viscosity (η) of each water−glycerol mixture are also indicated. These data show that a significant decrease of k_{nr} is observed with the increase in the medium viscosity, in agreement with previous results obtained for *o*-DASPMI in several *n*-alcohols.[22] These results indicate that, under these experimental conditions, it is of importance to examine the correlation between the medium's viscosity and k_{nr}, through the phenomenological (empirical) relationship[30]

$$k_{nr} = \frac{A}{\eta^x} \tag{8}$$

where A and x are parameters depending on the system. The log−log representation, shown in Figure 2, gives $x = 0.45$. This result indicates that the macroscopic viscosity is not appropriate to describe the microenvironment probed by *p*-DASPMI. In fact the free volume of the solvent mixture becomes a relevant parameter,[30] and thus the probe senses the solvent as a discontinuous medium. This behavior is understandable since the characteristic dimensions of the probe are most probably comparable to the mean free path in the host media. The approximate volume of *p*-DASPMI, as calculated using Hyperchem 7 software, is estimated to be on the order of 240 Å^3, by assuming a cylindrical shape.

A realistic approach to the hydrodynamics of *p*-DASPMI was obtained from time-resolved anisotropy measurements, performed as described in section 2.2. Table 3 shows the measured rotational correlation times (τ_r) and the initial anisotropy (r_0).

TABLE 2: Photophysical Parameters of *p*-DASPMI in Glycerol−Water Mixtures

sample composition (wt % Gly)	refractive index[a]	relative viscosity[a]	quantum yield[b]	average lifetime (ns)	k_f [c] (s^{-1})	k_{nr} [d] (s^{-1})
80	1.4431	59.78	0.038	0.250	1.52×10^8	3.85×10^9
84	1.4492	84.17	0.049	0.327	1.49×10^8	2.91×10^9
88	1.4553	147.2	0.062	0.439	1.42×10^8	2.14×10^9
92	1.4613	383.7	0.085	0.602	1.42×10^8	1.52×10^9
96	1.4674	778.9	0.100	0.775	1.29×10^8	1.16×10^9
100	1.4735	1759.6	0.241	1.03	2.34×10^8	7.37×10^8

[a] *Handbook of Chemistry and Physics*, 57th ed.; CRC Press: Boca Raton, FL. Viscosity data are relative to the viscosity of water at 20 °C ($\eta_0 = 1.002$ cP). [b] Measured relative to *p*-DASPMI in ethanol ($\Phi_{\text{DASPMI in ethanol}} = 0.008$).[16] [c] k_r = radiative rate constant. [d] k_{nr} = nonradiative rate constant.

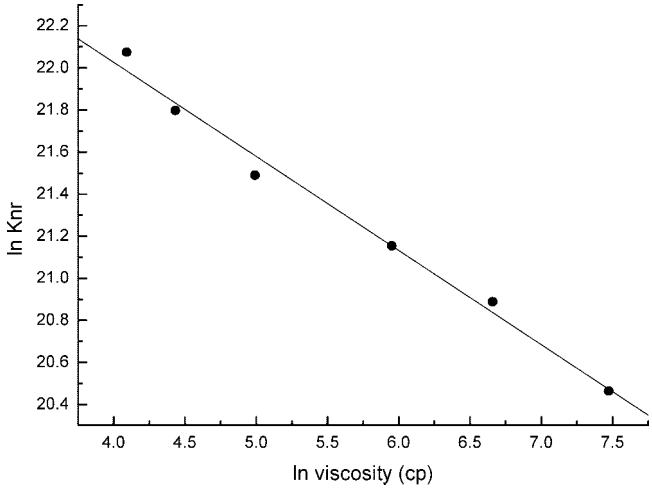

Figure 2. Correlation between the nonradiative constant of *p*-DASPMI emission and the host medium viscosity. Linear fit with a gradient of -0.45 ± 0.02. The goodness of fit (R) was 0.994.

TABLE 3: Time-Resolved Anisotropy Data of *p*-DASPMI in Glycerol−Water Mixtures and Hydrodynamic Parameters (Limiting Anisotropy, r_∞, Fixed as 0)

sample composition (wt % Gly)	τ_r (ns)	r_0	χ^2	η_{eff} [a] (cP)	V_H [b] (Å^3)	R_H [c] (Å)
84	3.2 ± 0.3	0.294	1.23	7.35	1791	7.5
88	5.7 ± 0.9	0.280	1.25	9.45	2481	8.4
92	16.0 ± 1.8	0.338	1.11	14.55	4525	10.3
96	15.6 ± 1.4	0.231	1.20	20.01	3208	9.1
100	38.9 ± 6.8	0.274	1.05	28.87	5544	11.0

[a] η = effective viscosity. [b] V_H = hydrodynamic volume. [c] R_H = hydrodynamic radius.

The limiting anisotropy (r_∞) was assumed to be zero throughout. The values found for r_0 indicate that a significant part of the initial decay is observed. However, the fact that the values of τ_r are somewhat longer than the fluorescence lifetimes (τ_f) precluded the measurement of the complete $r(t)$ decay function. Table 3 also includes the values for the hydrodynamic volume (V_H) and radius (R_H) of *p*-DASPMI in each solution. These values were obtained through eq 5, by assuming the effective viscosity

$$\eta_{eff} = (\eta_{bulk})^{0.45} \quad (9)$$

to be more suitable to describe the local environment probed by *p*-DASPMI in each solution. All values found for V_H were substantially higher than the approximate volume of *p*-DASPMI (~240 Å^3). These values show that the probe is firmly bound to solvent molecules (either glycerol or water). The positive charge of the dye molecule facilitates its interaction with the solvent molecules, thus promoting the "binding of a solvent cage" to each *p*-DASPMI molecule, which rotates along with the dye.

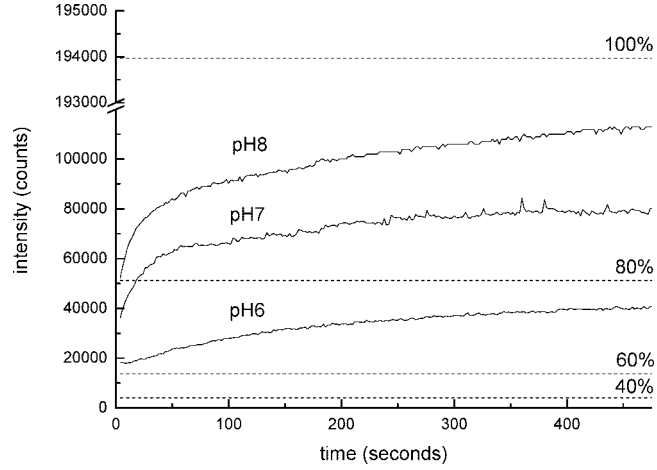

Figure 3. Effect of pH on gelation and initial aging of TEOS matrices probed through *p*-DASPMI steady-state emission. Excitation was at 490 nm with emission maxima at 600 nm. The intensity of DASPMI emission (under the same conditions) for different glycerol−water mixtures (percent glycerol shown) are indicated by the dashed lines.

3.2. Monitoring the Gelation and Initial Aging Phases. Because the authors' interests are related to the incorporation of proteins within SGMs, an initial study was performed producing matrices without the additional modifiers, at different pH values (pH 6, 7, and 8) in order to ascertain if this factor had any effect on the gelation process. The sol−gel reaction conditions are as we have reported previously,[27] and the pH values restricted to a range so as to not protonate the DASPMI, since this can lead to a spectral change,[23,26] as referred to in section 2.1.

The emission spectra of *p*-DASPMI, in all three media, are identical to the spectrum of *p*-DASPMI in water, measured under the same instrumental conditions, both in shape and in the energy corresponding to the emission maximum. In fact, all spectra are structureless, highly symmetrical, and centered at 600 nm. The results are shown in Figure 3, where the relative fluorescence intensity of *p*-DASPMI is shown as a function of time, during the gelation and initial aging processes. The intensity of the *p*-DASPMI emission (under the same conditions) for different glycerol−water mixtures (percent glycerol shown) is indicated as dashed lines. These results show that samples produced using higher pHs are more viscous. Moreover, the relative intensity of the *p*-DASPMI emission in TEOS suffers a drastic increase during the gelation process, for pH = 7 and pH = 8 solutions. The observed enhancement of ϕ_F is in

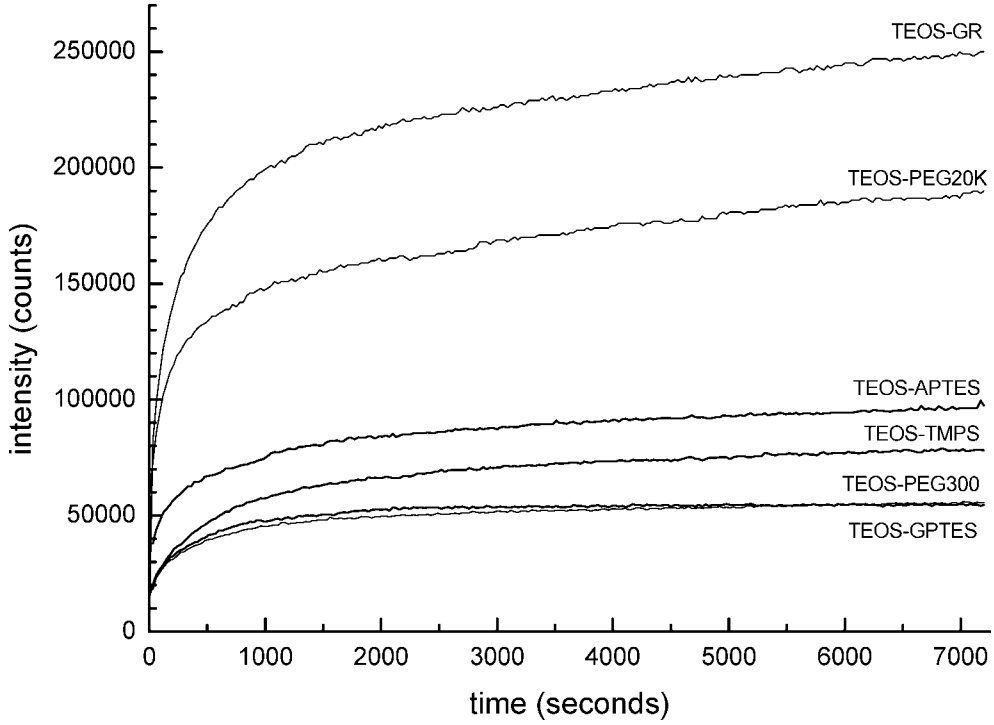

Figure 4. Intensity of *p*-DASPMI steady-state emission during the gelation and initial aging of modified samples. Excitation was at 490 nm with emission maxima at 600 nm.

agreement with the results obtained with water−glycerol mixtures and also with the work of Strehmel and Rettig.[22] These authors have reported a significant increase in ϕ_F and τ_F of *o*-DASPMI upon an increase in solvent viscosity. More recently, Ramadass and Bereiter-Hahn[19] observed a drastic increase in the emission lifetimes of *o*-DASPMI with an increase of solvent viscosity. The same study reports that the emission spectrum in polar media is very symmetrical, as opposed to the corresponding emission in nonpolar solvents, where the red-edge effect is quite visible. The data reported in this section confirm that, during the initial stages, the viscosity of all TEOS samples increases drastically and rapidly as the SiO_2 network starts to form and the sample changes from the liquid to the gel state. Afterward a more gradual increase in intensity is observed that corresponds to the initial aging phase. In all subsequent studies pH 7 was adopted.

The study on the gelation and initial aging phases was completed by examining the emission of the dye in the modified matrices during this process. The modifiers were either silanes (TMPS, APTES, and GPTES) or polymers (PEG 20*k*, PEG 300, and GR). Comparison of Figures 3 and 4 show that, in general, this process is significantly slower in the modified matrices, as compared with the nonmodified ones. This effect suggests a slower building up of the matrix structure, as caused by the presence of the modifiers. Examination of Figure 4 shows that the reaction is more extensive when GR or PEG 20*k* are present. These results are in agreement with the work of Shchipunov et al.,[31] thus confirming that polysaccharides enhance the polymerization of the SiO_2 network. GR is a polysaccharide with self-gelling properties composed of glucose, glucoronic acid, and rhamnose moieties.[32] It is probable that, when mixed with the sol, it favors the silica polymerization along its branches, thus explaining the highest intensity of the *p*-DASPMI emission in its presence. The results also suggest that the length of the polymer chain is important, since Figure 4 shows that PEG 300 has considerably less effect than PEG 20*k* in the building of the matrix network. The remaining modifiers (APTES, TMPS, and GPTES) do not significantly alter the gelation and initial aging processes, as can be seen by the comparison between the curves in Figure 4 and the gelation curve at pH 7 in Figure 3.

Therefore, these results show that *p*-DASPMI is an appropriate molecule with which to probe the deep changes that occur during the gelation and initial aging processes, in particular the drastic enhancement in the viscosity associated with the building of the matrix network.

3.3. Long-Term Monitoring of the Aging Process. The aging process was monitored during a period of over 40 days, in which the steady-state emission of *p*-DASPMI was measured periodically. Figure 5 shows the changes observed in the steady-state fluorescence of the dye with aging time. Difference spectra were obtained as described in section 2.2. These data show that, as the aging progresses, a slight blue shift is observed. This solvatochromic shift is reported by about 5% of the excited dye molecules in the TEOS−TMPS and TEOS−APTES samples, 10% in TEOS−GPTES, TEOS−PEG 20*k*, and TEOS−GR, and 20% in TEOS−PEG 300. The blue shift indicates that a

TABLE 4: Time-Resolved Fluorescence Data for DASPMI in the TEOS Matrix with pH 7 Buffer, through Aging

day	τ_1(ns)	τ_2 (ns)	τ_3 (ns)	α_1	α_2	α_3	χ^2
0	0.09 ± 0.06	0.96 ± 0.10	2.55 ± 0.03	0.78	0.17	0.05	1.09
1	0.10 ± 0.06	1.14 ± 0.09	2.79 ± 0.02	0.74	0.14	0.12	1.13
2	0.10 ± 0.09	1.13 ± 0.09	2.81 ± 0.02	0.69	0.15	0.15	1.05
3	0.19 ± 0.10	1.28 ± 0.11	2.90 ± 0.02	0.51	0.26	0.23	1.02
4	0.31 ± 0.20	1.43 ± 0.17	2.93 ± 0.03	0.41	0.28	0.32	1.10
6	0.19 ± 0.16	1.38 ± 0.15	2.94 ± 0.03	0.50	0.22	0.28	1.09
8	0.51 ± 0.23	1.80 ± 0.38	3.02 ± 0.05	0.35	0.27	0.38	1.08
11	0.56 ± 0.24	1.85 ± 0.31	3.08 ± 0.04	0.28	0.31	0.41	0.97
14	0.77 ± 0.46	1.89 ± 0.54	3.08 ± 0.05	0.24	0.29	0.47	1.08
17	0.41 ± 0.15	1.87 ± 0.36	3.14 ± 0.04	0.34	0.29	0.38	0.91
24	0.34 ± 0.24	1.73 ± 0.43	3.10 ± 0.03	0.22	0.26	0.52	1.06
29	0.64 ± 0.54	1.97 ± 0.12	3.16 ± 0.17	0.15	0.30	0.55	1.08
32	0.46 ± 0.14	1.99 ± 0.60	3.14 ± 0.05	0.22	0.26	0.52	1.09

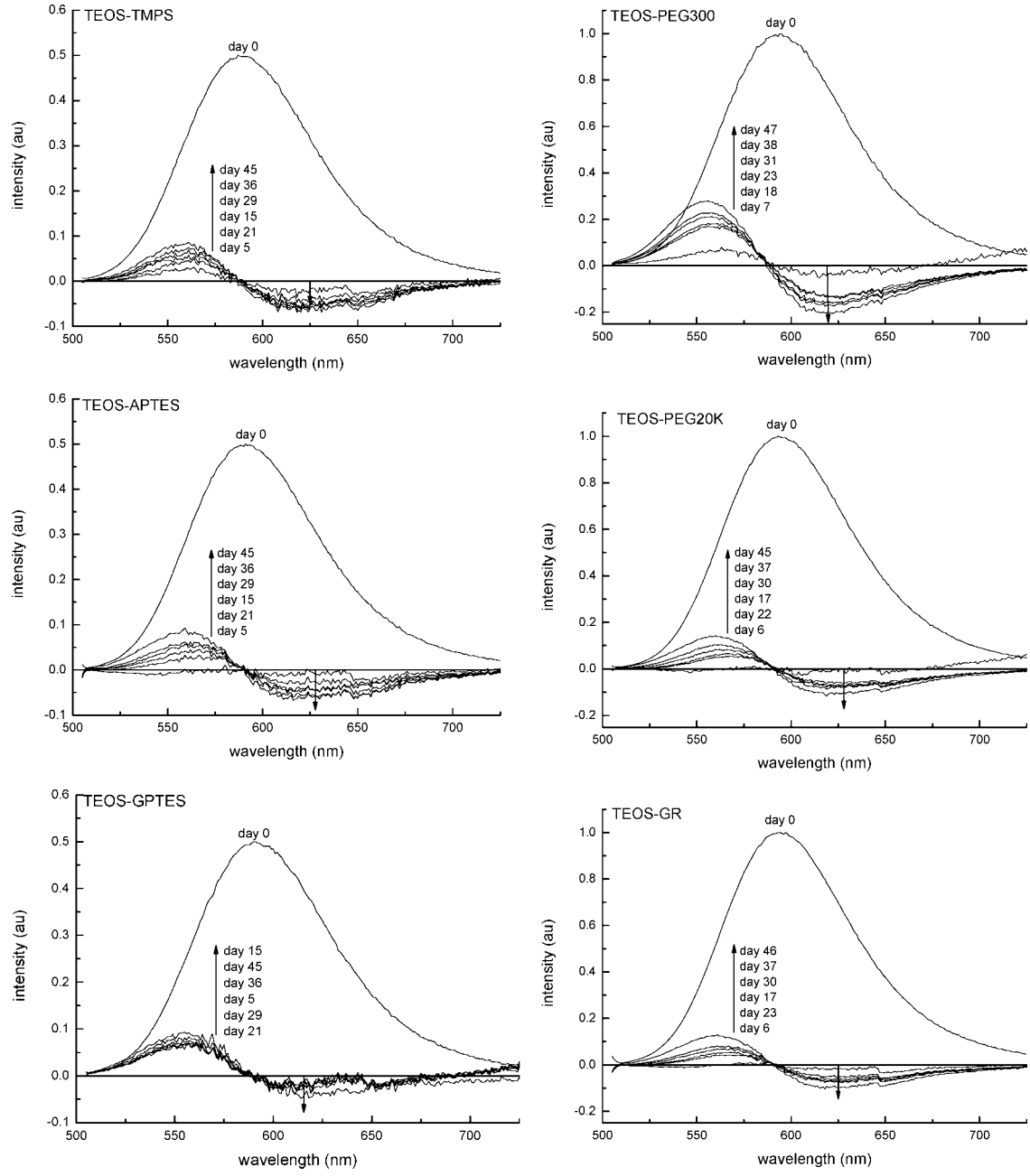

Figure 5. DASPMI steady-state emission at day 0 and difference spectra with aging time. Spectra were obtained by normalizing to unity at 600 nm and subtracting the spectrum for day 0. This spectrum is also shown reduced to half-height, for clarity, in the case of the samples TEOS−TMPS, TEOS−APTES, and TEOS−GPTES.

significant fraction (5−20%) of the dye molecules probes a slight decrease in the polarity of the host medium, favored by aging. This behavior is not surprising since the chemical composition of the liquid phase changes throughout the gel and aging processes. It is expected that not only water (the main component), but also some vestigial ethanol may remain in the liquid phase retained in the pores of the matrix network, formed as a byproduct of the polymerization of the silica. Moreover, the modifiers, a few remaining TEOS monomers, and other possible oligomers add to the complexity of liquid-phase chemical composition.

The aging process was further examined through extensive fluorescence lifetime measurements, as shown in Tables 4–10. These results show that the following general trends were found: (a) all decays can be adjusted to a three-component kinetics, (b) significant scatter in the values of the lifetimes can be found up to the 20th day, (c) the aging process appears to be more stable after the 20th day, (d) the longer lived component, a minor contribution in the early days, becomes more prominent as the aging process develops, and (e) all recovered lifetimes (τ_1, τ_2, and τ_3) increase with aging time. Moreover, it is generally observed that the relative contributions of τ_2 and τ_3 components become more important as the aging progresses, except for the TEOS−GPTES matrix (Table 7). In this case, not only the relative importance of each component is less obvious during the initial stages of the aging process but also, at the end of this process, the decrease of the percentage attributed to τ_1, e.g. α_1, is only somewhat lower than α_2 and α_3. Most probably, the GPTES modifier "templates" the building of the matrix network by allowing big pores[33] to be formed, thus providing the formation of important "solvent pools"; this hypothesis is

TABLE 5: Time-Resolved Fluorescence Data for DASPMI in the TEOS−TMPS Matrix, through Aging

day	τ_1 (ns)	τ_2 (ns)	τ_3 (ns)	α_1	α_2	α_3	χ^2
0	0.21 ± 0.08	1.23 ± 0.08	1.23 ± 0.03	0.65	0.23	0.12	1.03
1	0.19 ± 0.09	1.14 ± 0.08	2.66 ± 0.03	0.61	0.23	0.15	1.10
2	0.25 ± 0.10	1.32 ± 0.10	2.77 ± 0.03	0.58	0.26	0.16	1.06
5	0.15 ± 0.09	1.25 ± 0.09	2.75 ± 0.03	0.67	0.19	0.14	1.06
6	0.45 ± 0.18	1.45 ± 0.19	2.80 ± 0.04	0.43	0.31	0.26	1.09
7	0.30 ± 0.13	1.35 ± 0.11	2.79 ± 0.03	0.49	0.29	0.22	1.03
8	0.31 ± 0.15	1.35 ± 0.12	2.80 ± 0.03	0.49	0.28	0.23	1.06
9	0.14 ± 0.11	1.32 ± 0.09	2.80 ± 0.02	0.58	0.23	0.19	1.04
12	0.14 ± 0.11	1.32 ± 0.11	2.80 ± 0.03	0.67	0.18	0.15	1.08
13	0.24 ± 0.18	1.31 ± 0.11	2.82 ± 0.03	0.49	0.27	0.24	1.04
16	0.22 ± 0.13	1.34 ± 0.11	2.85 ± 0.03	0.50	0.27	0.23	1.13
21	0.59 ± 0.16	1.87 ± 0.37	2.97 ± 0.07	0.41	0.33	0.26	1.07
29	0.52 ± 0.18	1.61 ± 0.22	2.90 ± 0.04	0.38	0.30	0.32	1.09
35	0.49 ± 0.05	1.65 ± 0.06	2.96 ± 0.01	0.33	0.36	0.31	1.05
45	0.50 ± 0.17	1.66 ± 0.20	2.94 ± 0.04	0.36	0.32	0.32	1.07

TABLE 6: Time-Resolved Fluorescence Data for DASPMI in the TEOS−APTES Matrix, through Aging

day	τ_1 (ns)	τ_2 (ns)	τ_3 (ns)	α_1	α_2	α_3	χ^2
0	0.19 ± 0.05	1.34 ± 0.12	2.88 ± 0.03	0.62	0.21	0.16	1.06
1	0.23 ± 0.07	1.40 ± 0.20	2.91 ± 0.03	0.54	0.22	0.24	1.05
2	0.13 ± 0.09	1.31 ± 0.11	2.92 ± 0.02	0.64	0.17	0.19	1.10
5	0.50 ± 0.36	1.60 ± 0.30	3.00 ± 0.04	0.25	0.31	0.44	1.10
6	0.49 ± 0.25	1.76 ± 0.36	3.02 ± 0.04	0.29	0.28	0.43	1.08
7	0.05 ± 0.07	1.43 ± 0.15	2.98 ± 0.02	0.86	0.05	0.08	1.19
8	0.21 ± 0.18	1.39 ± 0.19	2.94 ± 0.02	0.45	0.19	0.36	1.09
9	0.51 ± 0.14	2.27 ± 0.27	3.30 ± 0.08	0.35	0.41	0.24	1.04
12	0.16 ± 0.27	1.62 ± 0.22	3.03 ± 0.03	0.57	0.16	0.28	1.10
13	0.58 ± 0.14	2.33 ± 0.30	3.31 ± 0.08	0.32	0.42	0.27	1.00
16	0.12 ± 0.10	1.50 ± 0.18	3.04 ± 0.02	0.55	0.15	0.29	1.08
21	0.71 ± 0.28	1.43 ± 0.14	3.00 ± 0.04	0.17	0.20	0.63	1.06
29	0.55 ± 0.28	2.00 ± 0.35	3.16 ± 0.04	0.21	0.3	0.49	1.07
35	0.71 ± 0.27	2.32 ± 0.47	3.25 ± 0.07	0.20	0.40	0.40	1.10
45	0.70 ± 0.42	2.07 ± 0.54	3.14 ± 0.05	0.19	0.28	0.53	1.06

TABLE 7: Time-Resolved Fluorescence Data for DASPMI in the TEOS−GPTES Matrix, through Aging

day	τ_1 (ns)	τ_2 (ns)	τ_3 (ns)	α_1	α_2	α_3	χ^2
0	0.25 ± 0.05	1.35 ± 0.23	2.81 ± 0.03	0.23	0.60	0.17	1.06
1	0.23 ± 0.07	1.40 ± 0.20	2.91 ± 0.03	0.54	0.22	0.24	1.05
2	0.72 ± 0.14	2.33 ± 0.16	3.78 ± 0.18	0.41	0.52	0.07	1.11
5	0.54 ± 0.22	2.12 ± 0.16	3.44 ± 0.09	0.37	0.49	0.14	1.05
6	0.50 ± 0.08	1.87 ± 0.40	3.06 ± 0.06	0.32	0.39	0.29	1.09
7	0.15 ± 0.09	1.46 ± 0.12	2.93 ± 0.03	0.54	0.24	0.23	1.02
8	0.62 ± 0.14	2.21 ± 0.17	3.47 ± 0.11	0.37	0.50	0.13	1.08
9	0.61 ± 0.16	2.21 ± 0.17	3.46 ± 0.11	0.36	0.50	0.13	1.07
12	0.49 ± 0.17	1.91 ± 0.20	3.10 ± 0.05	0.37	0.38	0.25	1.08
13	0.55 ± 0.13	2.14 ± 0.16	3.41 ± 0.09	0.37	0.48	0.15	1.03
16	0.60 ± 0.18	2.13 ± 0.20	3.32 ± 0.09	0.35	0.47	0.18	1.09
21	0.40 ± 0.18	1.78 ± 0.19	3.05 ± 0.04	0.37	0.35	0.28	1.17
29	0.67 ± 0.14	2.28 ± 0.19	3.48 ± 0.12	0.36	0.50	0.14	1.03
35	0.71 ± 0.22	2.07 ± 0.28	3.17 ± 0.07	0.29	0.43	0.28	1.06
45	0.60 ± 0.23	1.91 ± 0.26	3.07 ± 0.05	0.28	0.38	0.34	1.03

supported by the presence, in GPTES, of the relatively large/bulky glycidyloxypropyl group which does not bind chemically to the matrix network. Under these circumstances a very significant number of *p*-DASPMI molecules, by inhabiting these "large pools", become less sensitive to the matrix aging process. This is in agreement with the data on the early aging stages of the TEOS−GPTES matrix, shown in Figure 4. In fact, *p*-DASPMI, when in TEOS−GPTES matrix, reports the lowest increase in viscosity as compared to the other silane-modified matrices, thus confirming that the presence of GPTES induces the formation of a matrix with wide pores.

TABLE 8: Time-Resolved Fluorescence Data for DASPMI in the TEOS−PEG 300 Matrix, through Aging

day	τ_1 (ns)	τ_2 (ns)	τ_3 (ns)	α_1	α_2	α_3	χ^2
0	0.15 ± 0.07	1.05 ± 0.07	2.66 ± 0.03	0.70	0.19	0.11	1.07
1	0.11 ± 0.08	1.12 ± 0.08	2.74 ± 0.02	0.78	0.13	0.09	1.04
2	0.23 ± 0.07	1.39 ± 0.12	2.86 ± 0.03	0.66	0.19	0.15	1.06
3	0.23 ± 0.20	1.34 ± 0.12	2.84 ± 0.03	0.60	0.21	0.19	1.05
4	0.30 ± 0.04	1.47 ± 0.06	2.89 ± 0.01	0.55	0.23	0.22	1.11
7	0.52 ± 0.15	1.83 ± 0.29	3.03 ± 0.06	0.41	0.31	0.28	1.10
8	0.13 ± 0.09	1.33 ± 0.13	2.89 ± 0.02	0.66	0.15	0.19	1.06
9	0.39 ± 0.13	1.69 ± 0.21	2.99 ± 0.04	0.41	0.29	0.29	1.10
10	0.11 ± 0.09	1.26 ± 0.14	2.86 ± 0.02	0.69	0.13	0.18	1.08
11	0.31 ± 0.16	1.62 ± 0.18	2.99 ± 0.03	0.43	0.26	0.30	1.04
14	0.14 ± 0.09	1.34 ± 0.10	2.82 ± 0.02	0.57	0.21	0.22	1.04
15	0.58 ± 0.16	1.96 ± 0.26	3.04 ± 0.06	0.35	0.38	0.27	1.11
18	0.38 ± 0.16	1.78 ± 0.26	3.01 ± 0.04	0.37	0.26	0.38	1.10
23	0.19 ± 0.14	1.61 ± 0.20	2.98 ± 0.03	0.50	0.19	0.31	1.05
31	0.56 ± 0.21	2.10 ± 0.29	3.15 ± 0.05	0.24	0.39	0.37	0.97
37	0.66 ± 0.36	2.14 ± 0.44	3.12 ± 0.06	0.23	0.36	0.41	1.10
47	0.65 ± 0.32	2.10 ± 0.45	3.08 ± 0.05	0.19	0.33	0.47	1.05

TABLE 9: Time-Resolved Fluorescence Data for DASPMI in the TEOS−PEG 20*k* Matrix, through Aging

day	τ_1 (ns)	τ_2 (ns)	τ_3 (ns)	α_1	α_2	α_3	χ^2
0	0.24 ± 0.12	1.12 ± 0.10	2.67 ± 0.03	0.63	0.23	0.14	1.12
1	0.22 ± 0.09	1.26 ± 0.10	2.81 ± 0.03	0.62	0.22	0.16	1.12
2	0.15 ± 0.10	1.18 ± 0.09	2.81 ± 0.02	0.66	0.18	0.16	1.04
3	0.11 ± 0.08	1.31 ± 0.10	2.88 ± 0.03	0.74	0.13	0.12	1.04
6	0.13 ± 0.10	1.44 ± 0.11	2.95 ± 0.03	0.67	0.16	0.17	0.94
7	0.21 ± 0.31	1.42 ± 0.09	2.92 ± 0.03	0.22	0.51	0.28	1.06
8	0.69 ± 0.18	2.06 ± 0.46	3.11 ± 0.09	0.37	0.36	0.27	1.08
9	0.39 ± 0.13	1.69 ± 0.21	2.99 ± 0.04	0.41	0.29	0.29	1.10
10	0.21 ± 0.08	1.43 ± 0.16	2.93 ± 0.03	0.48	0.21	0.31	1.09
13	0.14 ± 0.14	1.28 ± 0.15	2.92 ± 0.02	0.57	0.16	0.27	1.08
14	0.47 ± 0.18	1.95 ± 0.25	3.14 ± 0.04	0.32	0.33	0.34	1.06
17	0.39 ± 0.20	1.91 ± 0.23	3.13 ± 0.04	0.32	0.32	0.36	0.98
22	0.44 ± 0.16	2.13 ± 0.27	3.22 ± 0.06	0.34	0.35	0.31	1.03
30	0.54 ± 0.23	1.97 ± 0.34	3.10 ± 0.04	0.23	0.31	0.46	1.01
36	0.86 ± 0.37	2.50 ± 0.55	3.32 ± 0.11	0.24	0.49	0.28	1.07
46	0.67 ± 0.32	2.04 ± 0.50	3.12 ± 0.05	0.19	0.28	0.53	1.11

TABLE 10: Time-Resolved Fluorescence Data for DASPMI in the TEOS−GGR Matrix, through Aging

day	τ_1 (ns)	τ_2 (ns)	τ_3 (ns)	α_1	α_2	α_3	χ^2
0	0.13 ± 0.05	1.06 ± 0.11	2.70 ± 0.03	0.73	0.16	0.10	1.10
1	0.22 ± 0.05	1.26 ± 0.16	2.81 ± 0.03	0.62	0.22	0.16	1.12
2	0.17 ± 0.07	1.32 ± 0.18	2.87 ± 0.03	0.64	0.19	0.17	1.13
3	0.11 ± 0.06	1.28 ± 0.13	2.87 ± 0.02	0.74	0.13	0.13	1.06
6	0.17 ± 0.12	1.43 ± 0.12	2.94 ± 0.03	0.58	0.20	0.22	1.09
7	0.17 ± 0.14	1.39 ± 0.13	2.93 ± 0.02	0.56	0.20	0.25	1.02
8	0.10 ± 0.07	1.39 ± 0.12	2.93 ± 0.02	0.73	0.12	0.15	1.07
9	0.15 ± 0.18	1.40 ± 0.14	2.93 ± 0.02	0.60	0.17	0.23	1.05
10	0.26 ± 0.43	1.36 ± 0.17	2.92 ± 0.02	0.39	0.24	0.37	1.08
13	0.26 ± 0.43	1.36 ± 0.17	2.92 ± 0.02	0.39	0.24	0.37	1.08
14	0.05 ± 0.07	1.24 ± 0.14	2.91 ± 0.02	0.82	0.07	0.11	1.11
17	0.48 ± 0.19	1.97 ± 0.26	3.15 ± 0.05	0.32	0.34	0.34	1.08
22	0.21 ± 0.15	1.50 ± 0.20	3.01 ± 0.02	0.43	0.20	0.37	1.08
30	0.62 ± 0.25	2.04 ± 0.37	3.14 ± 0.05	0.23	0.32	0.45	1.05
36	0.72 ± 0.28	2.21 ± 0.47	3.19 ± 0.07	0.23	0.35	0.42	1.09
46	0.65 ± 0.30	2.32 ± 0.42	3.27 ± 0.08	0.23	0.42	0.35	1.09

In summary, the time-resolved data point to the following conclusion: as the connectivity of the silica network increases during the aging process, *p*-DASPMI remains in the liquid phase retained within the pores. The aging process promotes the formation of the TICT state, thus confirming that the molecule can internally rotate (twist), unlike with the glycerol−water system. It is interesting to note that the systematic increase in the measured lifetimes indicates that the

liquid phase that hosts the dye becomes more viscous with aging, but the dye molecule remains free to reach the TICT state. Therefore, under these experimental conditions, the *p*-DASPMI emission reports on the polarity and hydrodynamic factors that characterize the evolution of the liquid phase in the hosts aging processes. These results indirectly point to the fact that the modifiers interact preferentially with the matrix network, as expected. In fact, the addition of silane modifiers is expected to alter the hydrophobic/hydrophilic balance of the interior of the pores, through capping unreacted OH groups, whereas the polymers are expected to adsorb onto the surface of the pores, decreasing the interaction of entrapped molecules with the silica wall in the pores.

4. Conclusion

In this work, time-resolved and steady-state fluorescence measurements of *p*-DASPMI were examined in order to monitor the profound changes that occur in the preparation of SGMs during the gelation and aging stages. It was possible to discriminate the dominant dye−host interactions in each of the main steps of the preparation of silane- and polymer-modified hosts. During the initial part of the gelation process *p*-DASPMI exhibits a drastic increase in quantum yield related to the increasing viscosity through the sol to gel transition, caused by a reduction in the nonradiative pathways. Over the next part of the process there is a high degree of scatter, in both the steady-state and time-resolved data, which is linked to DASPMI molecules encountering a range of environments before the structure of the media becomes more stable. Overall, the aging process stabilizes from day 20 onward. Changes in the peak steady-state emission most probably relate to alterations in the local polarity sensed by the probe, while the marked increase in intensity and lifetime values relate to decreased nonradiative deexcitation caused by increasing local viscosity. However, the viscosity enhancement does not prevent the formation of the TICT state, which is favored by the aging process. A complementary study on the photophysics of *p*-DASPMI in glycerol−water mixtures has provided evidence for the coexistence of hydrodynamic factors, expressed by a drastic decrease in nonradiative deactivation pathways and also for specific dye−host interactions, where hydrogen bonding within the solvent cage inhibits the formation of the TICT state in this system.

Acknowledgment. The Fundação para a Ciência e a Tecnologia is acknowledged for financial support through the Ph.D. Grant SFRH/BD/27933/2006.

References and Notes

(1) Hench, L. L.; West, J. K. *Chem. Rev.* **1992**, *90*, 33.
(2) Birch, D. J. S.; Geddes, C. D.; Karolin, J.; Leishman, R.; Rolinski, O. J. *Springer Ser. Fluorescence* **2002**, *2*, 69.
(3) Zink, J. I.; Dunn, B. *Chem. Mater.* **1997**, *9*, 2280.
(4) Gupta, R.; Mozumdar, S.; Chaudhury, N. K. *Biosensors & Bioelectronics* **2005**, *21*, 549.
(5) Unger, B.; Rurack, K.; Müller, R.; Jancke, H.; Resch-Genger, U. *J. Mater. Chem.* **2005**, *15*, 3069.
(6) Weber, G.; Farris, F. J. *Biochemistry* **1979**, *18*, 3075.
(7) Artukhov, V. Y.; Zharkova, O. M.; Morozova, J. P. *Spectrochim. Acta A* **2007**, *68*, 36.
(8) Greenspan, P.; Fowler, S. D. *J. Lipid Res.* **1985**, *26*, 781.
(9) Ghoneim, N. *Spectrochim. Acta A* **2000**, *56*, 1003.
(10) Flora, K. K.; Brennan, J. D. *J. Phys. Chem. B* **2001**, *105*, 12003.
(11) Viseu, T. M. R.; Hungerford, G.; Coelho, A. F.; Ferreira, M. I. C. *J. Phys. Chem. B* **2003**, *107*, 13300.
(12) Steiner, R. *Topics in Fluorescence Spectroscopy*; Lakowicz, J. R., Ed.; Plenum Press: New York, 1999; Vol. 2, pp 1−52. .
(13) Reits, A. J.; Neefjes, J. J. *Nat. Cell Biol.* **2001**, *3*, E145.
(14) Geddes, C. D.; Karolin, J.; Birch, D. J. S. *J. Fluorescence* **2002**, *12*, 135.
(15) Weiss, A. M.; Saraidarov, T.; Reisfeld, R. *Opt. Mater.* **2001**, *16*, 15.
(16) Hungerford, G.; Rei, A.; Ferreira, M. I. C.; Tregidgo, C.; Suhling, K. *Photochem. Photobiol. Sci.* **2007**, *6*, 825.
(17) Hungerford, G.; Rei, A.; Ferreira, M. I. C.; Suhling, K.; Tregidgo, C. *J. Phys. Chem. B* **2007**, *111*, 3558.
(18) Hellriegel, C.; Kirstein, J.; Brauchle, C.; Latour, V.; Pigot, T.; Olivier, R.; Lacombe, S.; Brown, R.; Guieu, V.; Payrastre, C.; Izquierdo, A.; Mocho, P. *J. Phys. Chem. B* **2004**, *108*, 14699.
(19) Ramadass, R.; Bereiter-Hahn, J. *J. Phys. Chem. B* **2007**, *111*, 7681.
(20) Yaffe, M. P.; Harata, D.; Verde, F.; Eddison, M.; Toda, T.; Nurse, P. *Proc. Natl. Acad. Sci. U.S.A.* **1996**, *93*, 11664.
(21) Goss, G. G.; Adamia, S.; Galvez, F. *Am. J. Physiol. Regul. Integr. Comp. Physiol.* **2001**, *281*, R1718.
(22) Strehmel, B.; Rettig, W. *J. Biomed. Opt.* **1996**, *1*, 98.
(23) Strehmel, B.; Seifert, H.; Rettig, W. *J. Phys. Chem. B* **1997**, *101*, 2232.
(24) Miller, E.; Wandelt, B.; Wysocki, S.; Jŏžwik, D.; Mielniczak, A. *Biosens. Bioelectron.* **2004**, *20*, 1196.
(25) Jŏžwik, D.; Miller, E.; Wandelt, B.; Wysocki, S. *Spectrochim. Acta. A* **2006**, *64*, 1125.
(26) Hungerford, G.; Pereira, M. R.; Ferreira, J. A.; Viseu, T. M. R.; Coelho, A. F.; Ferreira, M. I. C.; Suhling, K. *J. Fluorescence* **2002**, *12*, 397.
(27) Hungerford, G.; Rei, A.; Ferreira, M. I. C. *Biophys. Chem.* **2006**, *120*, 81.
(28) Demas, J. N.; Crosby, G. A. *J. Phys. Chem.* **1971**, *75*, 991.
(29) Dashnau, J. L.; Nucci, N. V.; Sharp, K. A.; Vanderkooi, J. M. *J. Phys. Chem. B* **2006**, *110*, 13670.
(30) Loutfy, R. O.; Arnold, B. A. *J. Phys. Chem.* **1982**, *86*, 4205.
(31) Shchipunov, Y. A.; Kojima, A.; Imae, T. *J. Colloid Interface Sci.* **2005**, *285*, 574.
(32) Shungu, D.; Valiant, M.; Tutlane, V.; Weinberg, E.; Weissberger, B.; Koupal, L.; Gadebusch, H.; Stapley, E. *Appl. Environ. Microbiol.* **1983**, *46*, 840.
(33) Lu, Y; Cao, G.; Kale, R. P.; Prabakar, S.; López, G. P.; Brinker, C. J. *Chem. Mater.* **1999**, *11*, 1223.

JP8013207